High-Resolution Soft-X-Ray Tomography of Sawtooth Oscillations on the Tokamak de Varennes

C. Janicki,[a] R. Décoste,[b] and C. Simm[c]
Centre Canadien de Fusion Magnétique, Varennes, Québec, Canada J0L 2P0
(Received 3 April 1989)

Up to five arrays of soft-x-ray detectors are used with the Fourier-Bessel harmonic reconstruction method to generate 2D images of sawtooth collapses during Ohmic plasma discharges on the Tokamak de Varennes. For low-harmonic reconstructions ($M \leq 2$), a quasi-interchange behavior (Wesson model) is observed during the sawtooth crash, but a reconnectionlike behavior (Kadomtsev model) is recovered using higher harmonics ($M \geq 3$) on the same data. This indicates that the Kadomtsev model is a better description for the sawtooth collapse, although the collapse time remains shorter than predicted.

PACS numbers: 52.55.Fa, 52.30.Jb, 52.35.Py, 52.70.La

Sawtooth oscillations[1] are internal disruptive instabilities observed on most tokamaks. This periodic phenomenon is observed on many plasma diagnostics and each cycle consists of a slow increase in the central temperature and density followed by a sudden collapse. As an explanation, Kadomtsev proposed the total reconnection model,[2] where an $m=1$ mode disappears nonlinearly through resistive reconnection at the $q=1$ surface, resulting in a flattening of the temperature, density, and current profile, and a release of energy. Detailed investigations using nonlinear two-dimensional codes[3-5] have shown that this model is consistent with MHD theory, and is able to explain several experimental observations on small tokamaks.[6-8] Recently though, this model has been called into question in the light of new experimental results obtained on large tokamaks.[9,10] The total reconnection model would fail to explain the fast sawtooth crash, and to a lesser extent, the lack of large precursors and the presence of large slowly decaying successor oscillations. A number of recent works have attempted to explain these new observations,[11-13] but most of the attention has been focused on the quasi-interchange (Wesson) model[13] since soft-x-ray-emission reconstructions on the Joint European Torus (JET) seem to agree with topological predictions of the sawtooth collapse phase.[14,15] In this model, a flattened q profile leads to an unstable $m=1$ mode, which drives a cold bubble toward the center of the plasma, expelling the initial hot core through an interchange mechanism. Qualitative differences between the total reconnection model and the quasi-interchange model should make clear experimental identification possible through tomographic imaging of soft-x-ray emission during the sawtooth collapse. In the total reconnection model, the hot core of the $q<1$ region moves almost rigidly to one side, whereas in the quasi-interchange model, the initial hot core becomes a crescent when the cold bubble penetrates the center region due to convective flow.[13] Despite such contrasting topological differences, experimental identification is not straightforward since spatial inversion techniques must be used to unfold line-integrated data obtained with discrete detectors. On tokamaks, several limitations on viewing angles and the number of detectors favor the Fourier-harmonic-reconstruction technique, which takes advantage of basic cylindrical symmetries. Typically, only two full projections or detector arrays are available, limiting the reconstructions to low-harmonic expansions, unless, as it is sometimes the case, rigid-body rotations can be assumed during relatively slow sawtooth crashes.[16] This paper shows that an analysis with a low-harmonic content is generally not sufficient to differentiate between the two sawtooth-collapse models and may even lead to erroneous conclusions should one model require a higher-harmonic content than the other for accurate reconstructions. Higher-harmonic reconstructions on the Tokamak de Varennes data indicate that the total reconnection model is a better topological description of the sawtooth collapse.[17]

The experiments reported here were performed on the Tokamak de Varennes, a medium-size machine with typical parameters $R=0.86$ m, $a=0.27$ m, $T_e=0.8$ keV, $T_i=0.5$ keV, and $B_T=1.5$ T. The measurements were performed on Ohmically heated plasmas, with current I_p ranging between 150 and 270 kA, a line-average electron density $\bar{n}_e$ between 2×10^9 and 4×10^{19} m^{-3}, and a minor radius set to $a=0.25$ m. The imaging system,[18] optimized for tomographic reconstructions, is shown schematically in Fig. 1(a). Five full projections of the plasma are available at one toroidal location. All detector channels are calibrated *in situ* to within 2% and the only energy filtering used in these experiments is a 25-μm Be window on the entrance slit of each array. A unique feature of this system lies in the excellent coverage of the (p,ϕ) space as shown in Fig. 1(c), with p and ϕ as defined in Fig. 1(b).

The Fourier-Bessel inversion method[19] is used to generate tomographic reconstructions from the soft-x-ray data. This method differs from the original Cormak inversion[20] in the radial expansion, using Bessel functions to replace the usual Zernicke polynomials. This choice yields better radial resolution in the central region and less spurious noise near the plasma edges, with the same

number of radial terms. In the polar coordinate system (r,θ), the signal from each detector is proportional to the x-ray chord brightness $f(p,\phi)$ (W cm^{-2} sr^{-1}), related to the local emissivity $g(r,\theta)$ (W cm^{-3}) through $f(p,\phi)=\int g(r,\theta)\,d\mathcal{L}$, with the integral performed along a line of sight $\mathcal{L}(p,\phi)$ of a detector through the plasma. The local emissivity $g(r,\theta)$ can be expanded in terms of Fourier harmonics to yield

$$f(p,\phi)=\sum_{m=0}^{M}\sum_{l=0}^{L}\int_{\mathcal{L}(p,\phi)}[a^{c}_{m,l}\cos(m\theta)+a^{s}_{m,l}\sin(m\theta)]g_{m,l}(r)\,d\mathcal{L}\,, \tag{1}$$

where $g_{m,l}(r)=J_m(\lambda_m^{l+1}r)$, and λ_m^l is the lth zero of the Bessel function $J_m(a)$. After numerical integration along the chords $\mathcal{L}(p,\phi)$, Eq. (1) can be put in a matrix form and inverted to obtain the $a_{m,l}$ coefficients and consequently the local emissivities. The main limitation of this technique comes obviously from the finite number of expansion terms that can be used in Eq. (1), giving the imaging system configuration. The radial expansion limit L, restricted by the chord spacing, is usually adequate. A much more severe limitation comes from the angular expansion limit M, which is restricted by the number of arrays. For example, only four harmonic terms can be determined with two detector arrays: $m=0$, $\cos(\theta)$, $\sin(\theta)$, and either (but not both) the $\cos(2\theta)$ or $\sin(2\theta)$ component. However, five arrays allow full $M=4$ reconstructions, although in practice $M=3$ is usually preferred in order to overdefine slightly the linear system of equations [Eq. (1)], and take advantage of spatial noise reduction through least-squares matrix inversion techniques.

A typical soft-x-ray signal is shown in Fig. 2(a) for $I_p=200$ kA. In general, plasmas with lower currents (150 kA) exhibit much higher levels of $m=1$ activity before and after the sawtooth crash, whereas higher currents (250 kA) show very little or no precursor and/or successor oscillations. Despite these differences in associated MHD activity, sawtooth crashes reconstructed for various plasma conditions exhibit similar behaviors during the collapse phase and appear to involve the same mechanism. A typical reconstruction is shown in Figs. 2(d)–2(l), using all five arrays and an $L=6$, $M=3$ expansion in Eq. (1). The hot core (region of high emissivity) is seen to move outward as a nearly rigid structure [Figs. 2(g)–2(h)] in agreement with the Kadomtsev model. Small regions of locally lower or higher emissivity next to the hot core [upper left in Fig. 2(h)] can be explained to some extent by spatial noise or artefacts of the reconstruction technique, as discussed below. Similary, the apparent crescent shape of the remaining highly

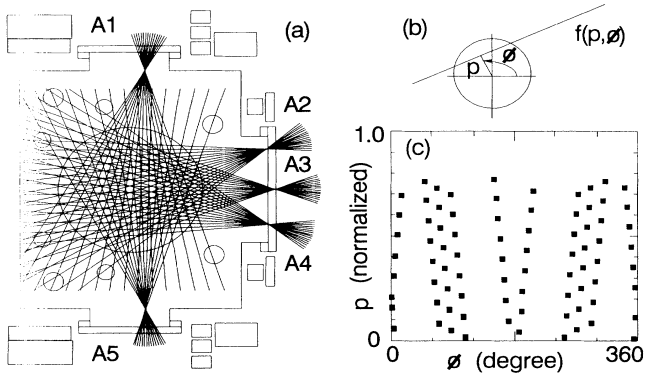

FIG. 1. (a) X-ray imaging system on the Tokamak de Varennes, with five arrays of sixteen silicon surface-barrier detectors each. (b) Coordinate system, where p is the chord impact parameter relative to the center of the reconstruction, ϕ is the polar angle, and $f(p,\phi)$ is the chord brightness. (c) Location of the detectors in the (p,ϕ) space. The coordinate p is normalized to unity for a minor radius $a=0.25$ m.

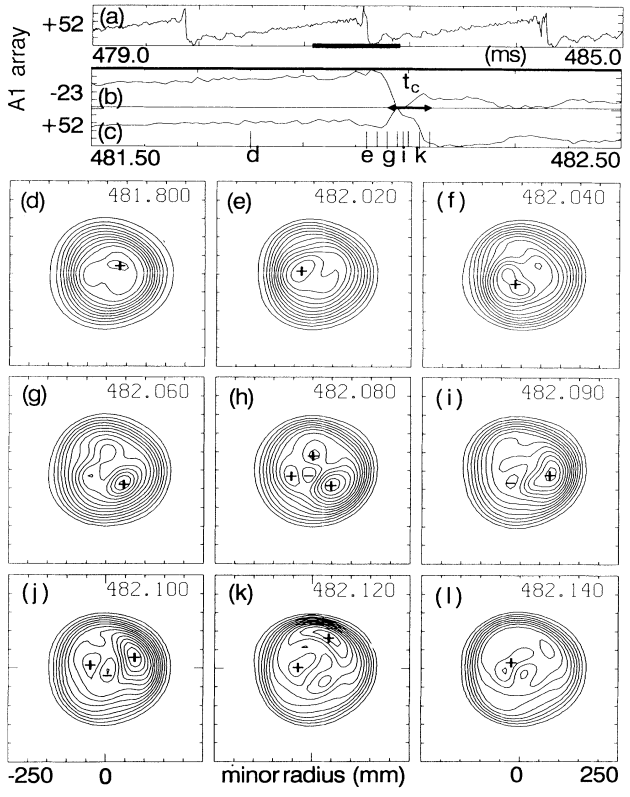

FIG. 2. (a) Soft x-ray signal (array $A1$, $p=52$ mm) exhibiting sawtooth activity. (b),(c) Time-expanded signals for chords respectively at $p=-23$ mm and $p=52$ mm (array $A1$). (d)–(l) Tomographic reconstructions using all five arrays and harmonics up to $M=3$ and $L=6$ as defined in Eq. (1). Regions of high and low emissivity are indicated with + and −, respectively. Plasma parameters (shot 5517): $I_p=200$ kA, $\bar{n}_e=3\times10^{19}$ m^{-3}, $a=0.25$ m.

displaced hot core in Fig. 2(k) is probably exaggerated and would most likely require much higher harmonics than $M=3$ for an accurate reconstruction.

Limitations of the reconstruction technique as a function of the harmonic content can be seen in the last two figures. Based on the same data (482.08 ms), Fig. 3 compares the $M=3$ reconstruction already shown in Fig. 2(h) with reconstructions using $M=1\frac{1}{2}$ [two arrays with full $m=1$ plus $\cos(2\theta)$] and $M=4$ (all five arrays). Even though all three reconstructions represent fairly good fits to the original data of the detector arrays [as seen in Figs. 3(d)–3(f) for array $A1$ only], the Akaike information criterion parameter[19] indicates that the goodness of the fit improves with higher M. The main conclusion of Fig. 3 is that the crescent shape of the displaced hot core inferred from the $M=1\frac{1}{2}$ reconstruction [Fig. 3(a)] becomes increasingly circular and the centered cold bubble gradually disappears as higher angular harmonics are used [Figs. 3(b) and 3(c)].

Further limitations of the reconstruction technique can be addressed through simulated reconstructions on various test functions using the actual detector geometry. Two examples are shown in Fig. 4. Both source functions were selected to yield simulated data profiles similar to the experimental profiles of Fig. 3. The first source function in Fig. 4(a) exhibits some qualitative features of the total reconnection (Kadomtsev) model (a relatively flat region in the center and a displaced circular hot core). The reconstructed image is seen to be highly distorted in Fig. 4(b) when using an $M=1\frac{1}{2}$ expansion (arrays $A1$ and $A3$ only), but improves significantly in Fig. 4(c) with $M=3$ expansion (all five arrays). Similarly, the second source function in Fig. 4(d), exhibiting some features of the quasi-interchange (Wesson) model (a cold bubble in the center and a crescent-shaped hot region), is reconstructed with $M=1\frac{1}{2}$ and $M=3$ in Figs. 4(e) and 4(f), respectively. It appears from these results that limiting the reconstructions to low harmonics ($M\leq 2$) artificially favors the quasi-interchange (Wesson) model since the sawtooth crash mechanism inferred from Fig. 4(b) would lead one to decide erroneously in favor of that model. This ambiguity can be lifted by using higher-harmonic reconstructions ($M\geq 3$) as seen in Figs. 4(c) and 4(f). The remaining differences between Figs. 4(a) and 4(c) suggest that small structures next to the hot core in Figs. 2(h)–2(j) could still be artefacts caused by limitations of the reconstruction technique. Other reconstructions with various source functions confirm that the level of artefacts increases with the relative strength of an off-center circular high-emissivity region, and that the reconstructed shape of the circular perturbation becomes increasingly elongated (crescent shaped) as it is moved outward, possibly explaining the topology of Fig. 2(k) as well.

We will now address the sawtooth crash time, t_c, defined in Fig. 2 as the time interval between the initial displacement of the hot core toward the $q=1$ surface [Fig. 2(e)] and its total collapse [Fig. 2(l)]. The crash time t_c has been measured for many plasma conditions (I_p and $\bar{n}_e$ ranging, respectively, from 150 to 270 kA and 2×10^{19} to 4×10^{19} m^{-3}) and found to vary typically from 80 to 160 μs with an average value around 110 μs. This is to be compared to the reconnection time given by

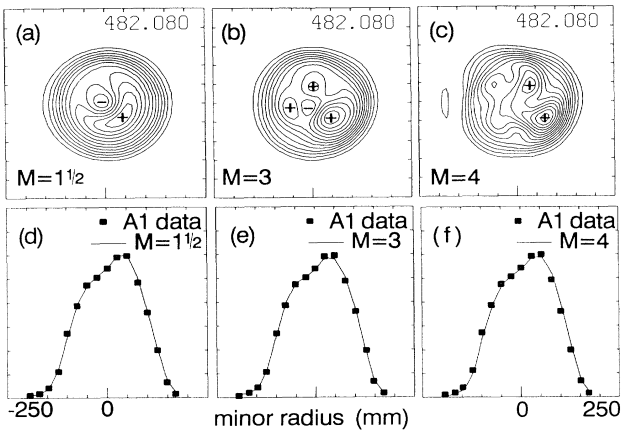

FIG. 3. Reconstructions using the same data set but different harmonic expansions. (a) Using arrays $A1$ and $A3$ only with $M=1\frac{1}{2}$ [including $\cos(2\theta)$ but not $\sin(2\theta)$], $L=6$. (b) Using all five arrays with $M=3$ and $L=6$ [same as Fig. 2(h)]. (c) All five arrays with $M=4$, $L=6$. (d),(e),(f) Fit to the data of array $A1$ from reconstruction (line integrals) shown in (a), (b), and (c), respectively.

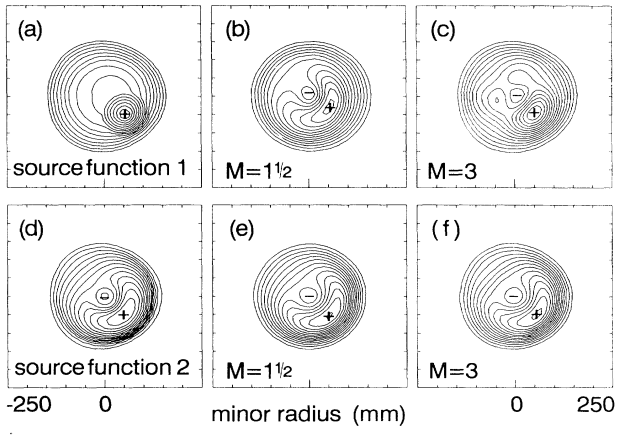

FIG. 4. Reconstruction of two test source functions with different harmonic contents. (a) Source function 1 exhibiting some features of the Kadomtsev model, with (b) $M=1\frac{1}{2}$, $L=6$ (arrays $A1$ and $A3$ only), and with (c) $M=3$, $L=6$ (all five arrays). (d) Source function 2 exhibiting some features of the Wesson model, reconstructed with (e) $M=1\frac{1}{2}$, $L=6$ (arrays $A1$ and $A3$ only) and with (f) $M=3$, $L=6$ (all five arrays).

the Kadomtsev model[2] $t_K=(\frac{1}{4}t_\eta t_A^*)^{1/2}$, where $t_\eta=\mu_0 \times r_1^2/\eta$ is the resistive diffusion time and $t_A^* =r_1(\mu_0\rho)^{1/2}/B^*$ is the modified Alfvén transition time in the helical magnetic field $B^*=(1-q_0)B_{p1}$. Here, r_1 is the radius of the $q=1$ surface, η is the Spitzer resistivity, ρ is the mass density, and B_{p1} is the poloidal field at $r=r_1$. The TSC code[21] has been used to determine B_{p1} and q_0, and consequently B^*. The range of plasma parameters given above yields $t_K\sim 650$–1000 μs (with $B^*=10^{-3}$ T), roughly an order of magnitude higher than the experimental value t_c. Much larger discrepancies have been reported on larger tokamaks.[9,10] It appears therefore that the experimental time scale for the sawtooth collapse phase is too fast when compared to the reconnection time given by the Kadomtsev model, although the observed topology of the sawtooth collapse is consistent with with this model.

In conclusion, this work demonstrates that the relatively low resolution in poloidal angle inherent in most tokamak soft-x-ray imaging systems strongly influences the tomographic reconstruction of complex phenomena such as sawtooth crashes. Reconstruction of the present observations using the number of poloidal harmonics appropriate to two angular viewing positions appears to exhibit a structure consistent with the quasi-interchange (Wesson) model. However, even if some fine details of the sawtooth collapse are still difficult to resolve with confidence, reconstruction using five angular viewing positions and higher harmonics reveals a structure more consistent with the total reconnection (Kadomtsev) model, although the observed crash time remains shorter than predicted.

The authors gratefully acknowledge the excellent technical assistance of P. Noël for the development and operation of the x-ray imaging system; M. Shoucri for providing the TSC code results; T. W. Johnston and H. D. Pacher for useful insights; and all the members of the Tokamak de Varennes team for continuous experimental support. The Centre Canadien de Fusion Magnétique is a joint project of Hydro-Québec, Atomic Energy of Canada Limited (AECL), and Institut National de la Recherche Scientifique (INRS) in which MPB Technologies, Inc., CANATOM, Inc, and the Université de Montréal also participate. It is principally funded by AECL, Hydro-Québec, and INRS.

[a]Also at MPB Technologies, Inc., Dorval, Québec, Canada.
[b]Also at Hydro-Québec, Varennes, Québec, Canada.
[c]Also at INRS-Energie, Varennes, Québec, Canada.

[1]S. von Goeler, W. Stodiek, and N. R. Sauthoff, Phys. Rev. Lett. **33**, 1201 (1974).
[2]B. B. Kadomtsev, Fiz. Plazmy **1**, 710 (1975) [Sov. J. Plasma Phys. **1**, 389 (1975)].
[3]A. Sykes and J. A. Wesson, Phys. Rev. Lett. **37**, 140 (1976).
[4]B. V. Waddel, M. N. Rosenbluth, D. A. Monticello, and R. B. White, Nucl. Fusion **16**, 528 (1976).
[5]A. F. Danilov, Yu. N. Dnestrovskii, D. P. Kostomarov, and A. M. Popov, Fiz. Plazmy **2**, 167 (1976) [Sov. J. Plasma Phys. **2**, 93 (1976)].
[6]G. L. Jahns, M. Soler, B. V. Waddel, J. D. Callen, and H. R. Hicks, Nucl. Fusion **18**, 609 (1978).
[7]W. Park, D. A. Monticello, and R. B. White, Phys. Fluids **27**, 137 (1984).
[8]R. S. Granetz and J. F. Camacho, Nucl. Fusion **25**, 727 (1985).
[9]D. J. Campbell, R. D. Gill, C.W. Gowers, J. A. Wesson, D. V. Bartlett, C. H. Best, S. Coda, A. E. Costley, A. Edwards, S. E. Kissel, R. M. Niestadt, H. W. Piekaar, R. Prentice, R. T. Ross, and B. J. D. Tubbing, Nucl. Fusion **26**, 1085 (1986).
[10]TFTR Group, K. McGuire *et al.* , in *Proceedings of the Eleventh International Conference on Plasma Physics and Controlled Nuclear Fusion Research, Kyoto, 1986,* edited by J. W. Weil and M. Demir (IAEA, Vienna, 1987), Vol. I, p. 421.
[11]R. G. Kleva, J. F. Drake, and R. E. Denton, Phys. Fluids **30**, 2119 (1987).
[12]A. Y. Aydemir, Phys. Rev. Lett. **59**, 649 (1987).
[13]J. A. Wesson, P. Kirby, and M. F. Nave, in Ref. 10, Vol. II, p. 3.
[14]A. W. Edwards, D. J. Campbell, W. W. Engelhardt, H.-U. Fahrbach, R. D. Gill, R. S. Granetz, S. Tsuji, B. J. D. Tubbing, A. Weller, J. Wesson, and D. Zasche, Phys. Rev. Lett. **57**, 210 (1986).
[15]R. S. Granetz and P. Smeulders, Nucl. Fusion **28**, 457 (1988).
[16]Y. Nagayama, S. Tsuji, and K. Kawahata, Phys. Rev. Lett. **61**, 1839 (1988).
[17]Y. Murakami, E. Fredrickson, and K. McGuire, Bull. Am. Phys. Soc. **33**, 2096 (1988).
[18]R. Décoste and P. Noël, Proc. SPIE Int. Soc. Opt. Eng. **661**, 50 (1986).
[19]Y. Nagayama, J. Appl. Phys. **62**, 2702 (1987).
[20]A. M. Cormack, J. Appl. Phys. **35**, 2908 (1964).
[21]S. C. Jardin, N. Pomphrey, and J. Delucia, J. Comput. Phys. **66**, 481 (1986).